FINAL TECHNICAL REPORT

External Grant award number 01HQGR0152

Title of Recipient's application:
One Decade of Strain in the Southern Cascadia Margin: Collaborative Research Between Humboldt State University and University of Alaska, Fairbanks

Title of Final Technical Report:
Contemporary GPS-derived strain in northern California: coastward escape of Sierra Nevada block motion contributes to southern Cascadia forearc contraction

Recipient's name: Harvey M. Kelsey

Program Element: Element II

Principle Investigators:

Todd B. Williams
Harvey M. Kelsey
Dept. of Geology
Humboldt State University
Arcata, CA 95521
707 826 3991; fax 707 826 5241
tbw3@axe.humboldt.edu
hmk1@axe.humboldt.edu

Jeffrey T. Freymueller
Geophysical Institute
University of Alaska
Fairbanks, AK 99775
907 474-7286
jeff@giseis.alaska.edu

Research supported by the U. S. Geological Survey (USGS), Department of Interior, under USGS award numbe 01HQGR0152. The views and conclusions contained in this document are those of the authors and should not b interpreted as necessarily representing the official policies, either expressed or implied, of the U. S. Government

Key Words: Neotectonics, Strain Measurements, GPS-Continuous, GPS-Campaign

TECHNICAL ABSTRACT for External Grant award number 01HQGR0152

Title of Recipient's Application:
One Decade of Strain in the Southern Cascadia Margin: Collaborative Research Between Humboldt State University and University of Alaska, Fairbanks

Title of Final Technical Report:
Contemporary GPS-derived strain in northern California: coastward escape of Sierra Nevada block motion contributes to southern Cascadia forearc contraction

Todd B. Williams; Harvey M. Kelsey
Dept. of Geology
Humboldt State University
Arcata, CA 95521
707 826 3991; fax 707 826 524
tbw3@axe.humboldt.edu; hmk1@axe.humboldt.edu

Jeffrey Freymueller
Geophysical Institute
University of Alaska
Fairbanks, AK 99775
907 474-7286
jeff@giseis.alaska.edu

TECHNICAL ABSTRACT

GPS-derived station velocities (1993-2002) in northwestern California reveal that processes other than subduction are in part accountable for observed upper plate contraction north of the migrating Mendocino triple junction (Mtj). Sites at and near Cape Mendocino are moving ~30 mm/yr and are consistently oriented approximately N 10° W, sub-parallel to the southern Cascadia trench. Sites just north of latitude 40.4° N begin to be oriented east of north, while stations ≥60 km north are consistently sub-parallel to the Gorda-North America plate convergence direction. North and east of Cape Mendocino, sites ~50-300 km inland have velocities oriented west of north, consistent with the direction of northern Sierra Nevada-Great Valley (SNGV) block and Pacific-North America (P-NA) relative motion. Northern SNGV block motion is ~11 mm/yr directed to the northwest. This velocity persists northwestward to within ~50 km of the coast at the latitude of Humboldt Bay. Approximately 20 mm/yr of distributed P-NA motion is observed inland of Cape Mendocino across the northern projections of the Maacama and Bartlett Springs fault zones. Approximately 8±2 mm/yr of P-NA motion is taken up as shortening in the upper plate of NA across the latitudinal region of the southern edge of the subducted Gorda plate. Approximately 10 mm/yr of the remaining P-NA motion continues northward into the Humboldt Bay region. The direction of observed SNGV block motion is obliquely convergent to the P-NA relative motion direction. Observed convergence of ~ 3 mm/yr occurs between the SNGV block and the Klamath Mountains beginning ~ 130 km inland of the coast near Weaverville, CA. Near Humboldt Bay, NE-SW convergence of ~ 14±2 mm/yr is observed from the coast to ~ 50 km inland. After removing an elastic dislocation model estimate of the interseismic subduction zone signal from the station velocities, convergence of inland stations with the Humboldt Bay region persists at ~3-7 mm/yr. Therefore, a significant portion of the upper plate contraction observed north of the Mendocino triple junction near Humboldt Bay is driven by convergence of the SNGV block with P-NA relative motion.

NON-TECHNICAL ABSTRACT for External Grant award number 01HQGR0152

Title of Recipient's application:
One Decade of Strain in the Southern Cascadia Margin: Collaborative Research Between Humboldt State University and University of Alaska, Fairbanks

Title of Final Technical report:
Contemporary GPS-derived strain in northern California: coastward escape of Sierra Nevada block motion contributes to southern Cascadia forearc contraction

Todd B. Williams; Harvey M. Kelsey
Dept. of Geology
Humboldt State University
Arcata, CA 95521
707 826 3991; fax 707 826 5241
tbw3@axe.humboldt.edu; hmk1@axe.humboldt.edu

Jeffrey Freymueller
Geophysical Institute
University of Alaska
Fairbanks, AK 99775
907 474-7286
jeff@giseis.alaska.edu

NON-TECHNICAL ABSTRACT

Global Positioning System (GPS) survey data from 1993 to 2002 provide estimates of tectonic deformation of North America in northernmost California. This region experiences stress from three different sources, the northern San Andreas fault system, which separates the North America and Pacific plates; the southern Cascadia subduction zone, which separates the Gorda and North America plates; and the northwestward encroachment of the Sierra Nevada-Great Valley block upon the Klamath Mountains and the coastal regions of northern California. From repeated periodic GPS surveys, these data indicate the northernmost projections of the San Andreas fault system are active and have measurable relative motion occurring across them. In addition, encroachment of the Sierra Nevada -Great Valley block may contribute up to half (2-4 mm/yr) of the observed geologic rate (~ 10 mm/yr) of shortening that occurs in the Humboldt bay area north of the Mendocino triple junction.

Introduction

The southern segment of the Cascadia margin is the only segment of the margin where active upper plate thrust faults within the deformation front are on-land. The Little Salmon and the Mad River fault zones trend approximately normal to the Gorda plate convergence direction and are evidence of late Quaternary contraction of the North American margin (Clarke and Carver, 1992). Strike-slip faults of the northern end of the San Andreas fault system trend northwesterly into the fold and thrust belt from the south (Kelsey and Carver, 1988) (Figure 1). Upper plate deformation at the southern Cascadia margin indicates that a portion of the convergence of the Gorda and North America plates is accommodated by internal shortening of North America, and the rest of the convergence being accommodated by slip on the subduction zone megathrust.

Despite assessment of geologic slip rates for active faults over the time frame of hundreds to thousands of years (Kelsey and Carver, 1988; Clarke and Carver, 1992), there are limited studies in northern coastal California on modern rates of deformation in the North American plate on a time scale of months to years. The presence of active crustal faults in the forearc implies that elastic deformation associated with upper plate faults, the plate interface, and the northern end of the San Andreas fault system contribute to the instantaneous velocity field measured by Global Positioning System (GPS) geodesy.

Through repeated periodic GPS surveys, this study provides an image of recent deformation (1993-2002) occurring near the Mendocino triple junction (Mtj) region and the southernmost segment of the Cascadia subduction zone (Csz). These measurements help evaluate: 1. The pattern of long term distributed deformation related to the broad P-NA plate boundary and the northward migration of the Mtj; 2. The interaction of P-NA plate boundary deformation with the southern Cascadia subduction zone; and 3. The rate of strain accumulation at coastal regions above the locked Cascadia megathrust.

GPS Geodetic Survey

This study builds upon initial GPS observations collected by the California Department of Transportation (CalTrans)(1993, 1994, 1998), the National Geodetic Survey (NGS)(1994, 1998), Stanford University (1994, 1995; Freymueller et al., 1999) and the U. S. Geological Survey (1996, 1999; Poland et al., 1999; J.Svarc, 2001, personal communication). Original data come from new observations made in 1999-2002. Processing follows procedures summarized in the Appendix. Most benchmarks resurveyed in this study are those of the California High Precision Geodetic Network (HPGN) jointly established in 1991 by CalTrans and the NGS.

GPS-derived station velocities (1993-2002) from 71 sites in North America help characterize deformation in northern coastal California and surrounding regions relative to stable North America (Table A). Average station velocity uncertainties are ~ 2 mm/yr (east-west) and ~1 mm/yr (north-south) at the 2-sigma (95%) confidence interval.

Observed Velocities in Northern California

Geologic provinces peripheral to northern coastal California have GPS station velocities characteristic of a broadly deforming plate boundary zone (Figure 1). The northern Basin and Range velocity is 3.4 ± 0.6 mm/yr west-northwest (SHLD; Figure 1). Stations east of the Sierra Nevada near the western Basin and Range and northern Walker Lane regions display 6.5 ± 0.5 mm/yr of northwest motion from near Honey Lake, CA across the southern Cascade volcanic arc (SHIN and YBHB; Figure 1). The northern Sierra Nevada and Great Valley (SNGV) are moving 10.8 ± 0.5 mm/yr northwest (QUIN and SUTB; Figure 1). This rate of motion is equal to values presented by Prescott et al. (2001) (10.7 ± 0.4 mm/yr) for stations that cover much more of the SNGV region. The magnitude of the station velocities observed in the northern Sierra Nevada and Great Valley are ~ 3 mm/yr less than the best fitting average Sierra-Nevada rigid block motion estimates presented by Dixon et al. (2000). However, the majority of sites that define Sierra-Nevada rigid block motion in Dixon et al. (2000) are significantly further south than stations QUIN and SUTB. The eastern Klamath Mountains and the southernmost western Cascade volcanic arc region are moving northwest to north at 7.1 ± 1.1 mm/yr. The western Klamath Mountains are moving north-northwest to due north at 9.7 ± 1.9 mm/yr. Both groups of

stations (western Klamath Mountains and eastern Klamath/western Cascade arc) display northwest-directed motion progressing to due north motion from south to north (Figure 2A).

In the region from the Mtj to Humboldt Bay, geodolite and GPS baseline measurements (1981-1989, 1991, 1992) indicate a complex transition from ~ 25 mm/yr of right-lateral shear south of Cape Mendocino to ~ 15 mm/yr of northeast directed uniaxial contraction north of Cape Mendocino (Murray et al., 1996). The developing northern end of the San Andreas fault zone is mapped at the surface to just south of the latitude of Cape Mendocino (Kelsey and Carver, 1988). Relative GPS station motion from Cape Mendocino eastward to ~ 80 km inland is 22.0 ± 1.1 mm/yr (CME1 to 0106; Figure 2), equivalent to the ~ 25 mm/yr from previous studies (Murray et al., 1996), and approximately half of the ~ 40-41mm/yr of P-NA relative motion observed within the Coast Ranges north of the San Francisco Bay region (Freymueller et al., 1999).

Incrementally increasing station velocity along latitude ~ 40.4° N spatially corresponds to three major fault zones of the northern San Andreas system. These are, east to west, the Bartlett Springs-Lake Mountain fault zone to the east, the Maacama-Garberville fault zones, and the San Andreas fault zone. Observed relative motion across the Lake Mountain fault zone of 6.4 ± 3.4 mm/yr is less than half of the ~ 8 mm/yr of fault slip determined by Freymueller et al. (1999) further south across the Bartlett Springs fault zone. Freymueller at al. (1999) determined ~ 14 mm/yr of slip occurs across the Maacama fault zone, much larger than the observed relative motion of ~ 5.3 ± 3.5 mm/yr across its projection, the northern Garberville fault zone. At 40.4° N, the relative station motion across the northern Lake Mountain fault zone and the northern Garberville fault zone are similar, whereas further to the south, the dextral slip fault zone closest to the Pacific plate has larger interseismic displacements (Freymueller et al, 1999). Equivalence of relative motion of the northern Lake Mountain fault zone and the northern Garberville fault zone suggests dextral deformation is currently concentrated across the Lake Mountain fault zone in the east, but deformation is distributed at the northern end of the Garberville fault zone; this inference is consistent with the field observation that the Lake Mountain fault zone can be clearly traced on the ground at latitude 40.4° N, whereas there is no clear field trace of the northern end of the Garberville fault zone (Kelsey and Carver, 1988).

GPS stations ~ 20-40 km north of latitude 40.4° N begin to have velocities oriented east of north, sub-parallel to the Gorda-North America convergence direction at a rate of ~ 10-15 mm/yr (Figure 2A). These rates are consistent with (but slightly greater than) previous USGS trilateration and GPS survey data within the southern Cascadia subduction zone (Murray et al., 1996; Murray and Lisowski, 2000) that show strain rates and magnitudes consistent with a megathrust slipping at the plate convergence rate, but locked at shallow depths. Northeast directed station velocities north of Cape Mendocino decrease northward. Along the coast, station velocities decrease from 31.1 ± 0.5 mm/yr at Cape Mendocino (CME1) to 17.2 ± 0.6 mm/yr at Trinidad (TRND) and to 12.1 ± 0.6 mm/yr at Crescent City (PTSG)(Figure 2A). Stations at and near Cape Mendocino are consistently oriented ~ N 10° W, sub-parallel to the trend of the southern Csz trench, whereas coastal stations at and north of Trinidad, CA (TRND) are consistently oriented ~ N 20-30° E, sub-parallel to Gorda-North America convergence. The azimuths of coastal stations at and north of Trinidad are consistent with the average P-axes orientations determined (~ 022°; Smith et al., 1993) from North America plate earthquakes recorded within the Humboldt Bay Seismic Network (1974-1984).

North of Cape Mendocino, inland stations converge upon coastal stations (Figure 2A). At latitude ~ 40.8° N, inland stations moving northwest sub-parallel to the Sierra Nevada block are as close as ~ 50 km to the coastline. The region separating inland northwest-directed velocities from coastal northeast-directed velocities marks the boundary between subduction dominated interseismic strain at the coast and translational strain of the interior southern Klamath Mountains. The SNGV block is converging upon the Klamath Mountains at a rate of ~ 3 mm/yr; the Klamath Mountains being at the northwest end of the P-NA velocity field. Observed convergence of coastal stations with stations ~ 50 km inland is ~ 14 ± 2 mm/yr. Rates of contraction north of Cape Mendocino (~ 15 mm/yr) determined from trilateration and GPS surveys (Murray et al., 1996; Murray and Lisowski, 2000; this study) agree with geologic rates of contraction of the upper plate of North America

across the fold and thrust belt in the Humboldt Bay region (≥ 10 mm/yr; Kelsey and Carver, 1988; McCrory, 2000).

Velocities with Subduction Zone Removed

The observed velocities (1993-2002) represent composite deformation associated with the northward migrating Mendocino triple junction, the San Andreas fault system, the southern Cascadia subduction zone, and upper plate faults within North America. A dislocation model of the subduction zone (Flueck et al., 1997) is used to remove one component of the composite deformation, the component of interseismic strain caused by a locked Cascadia subduction zone in northern California, allowing evaluation of other tectonic signals that contribute to deformation.

In utilizing the 3D-elastic dislocation model to estimate interseismic shortening along the northern California coast, the model geometry, locked zone, and transition zone determined for the Cascadia subduction zone as a whole (Flueck et al., 1997) are maintained for the southern end of the Cascadia margin, including the default locked and transition zone widths of 50-km each. The plate convergence rate (30 mm/yr) and azimuth (046°) used in the model are appropriate for the southern Cascadia margin (Miller et. al., 2001). The model is calculated at each GPS station location (Table B) and the resultant modeled station velocities, which reflect interseismic strain accumulation, are northeast-directed with a maximum of 12 mm/yr at Cape Mendocino.

An estimate of deformation that occurs within the North American plate and the San Andreas fault system is the residual velocity field (Figure 2B; Table C), computed by subtracting the modeled interseismic velocities from the observed velocities. The residual velocities in the far-field at stations removed from the subduction zone are essentially the same as the observed GPS velocities (compare Figures 2A and 2B) because far field stations are too far inland to be affected by interseismic strain above the locked portion of the subduction zone.

The residual velocities (Figure 2B), which are a composite sum of the deformation not recovered after each subduction zone earthquake, include elastic strain from thrust faults in the upper plate, influence of the San Andreas fault system, errors in the model, and measurement error. Most stations show residual velocities that are sub-parallel to the San Andreas fault system and related Sierra Nevada block motion, reflecting the influence of the Pacific-North America plate boundary on the southern Cascadia subduction zone.

Cape Mendocino region. The Cape Mendocino region is moving sub-parallel to the Pacific-North American relative plate motion direction (~ 26 mm/yr; Figure 3) at approximately half the observed rate (~ 47 mm/yr) of a station west of the San Andreas fault at Pt. Reyes, CA (PTRB, Figure 1). The distributed right-lateral motion (14.6 ± 1.1 mm/yr) occurring between Cape Mendocino and station 0106 (Figure 3), approximately 80 km inland from the coast, is approximately half the relative motion observed (32.5 ± 1.1 mm/yr) between Point Reyes (PTRB, Figure 1) and Sutter Buttes, CA (SUTB, Figure 1), suggesting a substantial amount of displacement is occurring offshore at the latitude of Cape Mendocino. The residual station velocities at latitude ~ 40.4° N (between CME1 and 0106; Figure 3) show the same westward increases as the observed velocities (Figure 2A). This gradient, while it may represent a gradual increase in northwest-directed translational strain, more likely can be accounted for by right-lateral strain on mapped north-northwest-trending faults (Figure 3). For Cape Mendocino and stations inland to the east, residual station velocities decrease rapidly along a northwest trend north of latitude 40.4° N, coincident with the southern edge of the subducted and internally deforming (Smith et al., 1993; Wilson, 1993) Gorda plate. Averaging the difference of three pairs of (NW-SE oriented) sites across this zone results in ~ 8 ± 2 mm/yr of NW-SE shortening (Figure 3) across the 40.4° N latitudinal region of the southern edge of the Gorda plate beneath North America.

Upper-plate thrust faults. Even after removing the modeled interseismic subduction zone velocities from the GPS velocities in the zone of upper plate contraction, individual GPS stations converge across mapped upper plate thrust faults (Figures 2B, 3 and 4). Considering GPS baselines with respect to station KNEE, centrally located in the zone of upper plate contraction (Figure 4), stations to the east of KNEE are converging upon stations west of KNEE at ~ 4-5 ± 2 mm/yr, with the ~ 4-5 ± 2 mm/yr velocity normal to mapped upper-plate

thrust faults near Humboldt Bay. Although sites inland are converging upon the coast, convergence of stations within the Mad River fault zone cannot be detected (Figure 4).

Margin-parallel contraction. The approximate 9.0 ± 5.0 mm/yr shortening parallel to the P-NA margin parallel motion between the Trinidad area (stations ALEN and TRND) and stations inland of Cape Mendocino (stations 01ND and 01NE) (Figure 4) is similar to (~ 8 ± 2 mm/yr), although more uncertain, than the three pairs of NW-SE situated stations presented in Figure 3. These rates of shortening are comparable to observed rates of shortening for the Puget Sound lowland (Miller et al., 2001) and the Los Angeles basin (Argus et. al., 1999). This contraction may be accommodated (as subsequent crustal thickening) locally as vertical deformation on high angle reverse faults near and immediately north of the triple junction region (e.g. Russ fault, Capetown fault) and/or as oblique reverse motion along the upper plate thrust faults (e.g. Mad River and Little Salmon fault zones). North-south shortening may also occur on long wavelength, east-west trending folds such as the Trinidad anticline (Kelsey and Carver, 1988; McCrory, 2000).

Convergence of Sierra Nevada-Great Valley block toward coast. Stations greater than 200 km inland of the coastal San Andreas transform zone, within the northern Sierra Nevada-Great Valley block, display velocities oriented slightly westward of the Pacific-North American relative motion direction until just north of the latitude of the triple junction region. Convergence of SNGV block motion with P-NA relative motion results in a zone of contraction that starts approximately 130 km east of the coast at station 0217 near Weaverville, CA (Figures 3 and 4) and persists westward into the Humboldt Bay region where it is influenced locally from motion fed from the Maacama and Bartlett Springs fault zones. The western edge of the contraction is manifest both in the geologic record of upper plate thrust faults of the Little Salmon and Mad River fault zones (Kelsey and Carver, 1988), and in the converging GPS-derived velocities across these fault zones (Figure 4). The rate of contemporaneous contraction deduced from residual velocities is approximately half the geologic contraction rate (≥ 10 mm/yr; Kelsey and Carver, 1988) across the Little Salmon and Mad River fault zones. Similarly, in the San Francisco Bay area >300 km south, the western edge of the Sierra Nevada-Great Valley block is converging at approximately 2-4 mm/yr with the eastern San Andreas fault system (Prescott et al., 2001).

The westerly directed velocities of SNGV reflect an escape of dextral, translational strain toward the coast contributing to localized upper plate contraction in northernmost coastal California. Development of permanent deformation in the upper plate near the coast is therefore in part a product of the impinging western edge of the Sierra Nevada-Great Valley block.

Conclusions

Based on GPS-derived station velocities (1993-2002), rates of deformation immediately south of the Mendocino triple junction are approximately 30 mm/yr directed to the northwest, whereas stations ≥40 km north of the Mendocino triple junction are moving approximately 10-15 mm/yr to the northeast. The transition zone from the northern SAF system begins across the Eel River Valley (station 01PA), and may be coincident with the southernmost active thrust faults within the upper plate (near station 01PB). GPS velocities sub-parallel to Gorda-North America convergence are consistently observed beginning immediately south of Trinidad, CA (TRND). This indicates that the transition from predominately translational strike-slip to predominately convergent subduction tectonics occurs over an ~ 80 km distance from the Eel River delta in Ferndale, CA to Trinidad, CA.. This transition zone experiences both types of deformation, strike-slip inland and contractional near the coast (Kelsey and Carver, 1988).

Using an elastic dislocation model to remove subduction-derived interseismic velocities from the observed GPS-derived velocities, P-NA relative motion persists as much as ~ 40 km north of the latitude of the offshore Mendocino fault. Pacific-North America relative motion at Cape Mendocino (26.2 ± 0.6 mm/yr) is approximately half that observed at Pt. Reyes (46.6 ± 2.0 mm/yr) near San Francisco, consistent with its position east of the San Andreas fault. Progressive westward increases in station velocities at the latitude of Cape Mendocino reflect dextral shear across the inland fault strands of the northernmost San Andreas fault zone. Station velocities increase across the northern Lake Mountain fault zone (6.4 ± 3.4 mm/yr) and across the

northward projection of the Garberville fault zone (5.3 ± 3.5 mm/yr) (Figure 3). The observed relative station motion is more concentrated in the vicinity of the Lake Mountain fault zone and more distributed in the west near the northern Garberville fault zone.

Northern Sierra Nevada-Great Valley block motion is ~ 11 mm/yr directed to the northwest and continues northwest to within ~50 km of the coast at the latitude of Humboldt Bay. The direction of Sierra Nevada-Great Valley motion is obliquely convergent to the Pacific-North America relative motion direction. Convergence of Sierra Nevada-Great Valley motion with the Klamath Mountains and the Coast Ranges begins ~ 130 km inland of the coast near Weaverville, CA (station 0217) (Figures 3 and 4). Even after removing the interseismic velocities, the northwestern end of the SNGV block, acting through the Klamath Mountains, converges to within ~ 50 km of the coast. The convergence of the northwestern edge of the Sierra Nevada-Great Valley block with the coastal regions therefore accounts for a portion of the observed contraction occurring north of the migrating Mendocino triple junction region. Upper plate contraction north of the Mendocino triple junction region near Humboldt Bay is driven not solely by Gorda-North America convergence, but in part by convergence of the Sierra Nevada-Great Valley block with coastal Pacific-North America relative motion. In addition, coastal northern California undergoes margin parallel shortening above the southern edge of the subducted Gorda plate.

Appendix: Data Analysis and North American Reference Frame

GPS phase data from the southern Csz and continuous stations in the surrounding area were processed using the GIPSY/OASIS II software (Zumberge et al., 1997). Analysis procedures are described in Freymueller et al. (1999, 2000). For data prior to 1995, global solutions were used to estimate satellite orbits, station coordinates, and noise parameters. For data collected since 1995, the NASA Jet Propulsion Lab (Pasadena, CA) non-fiducial orbits (Zumberge et al., 1997) were used to estimate station coordinates and noise parameters. For post-1995 solutions, a subset of the available continuous stations that span much of North America are included. The pre-1995 solutions are the same as those used in Freymueller et al. (1999), with a few reprocessed with newly available data.

Each individual solution is transformed into the International Terrestrial Reference Frame (ITRF97)(Boucher et al., 1999) evaluated at the epoch of the solution. Each solution contains continuous stations that have precise positions and velocities in the ITRF. Each station is weighted by the combined uncertainty of its position in the ITRF and uncertainty in the solution produced from this study. After transformation, solution agreement with ITRF97 is about 6 mm three-dimensional root mean square. Transformed solutions are used to estimate velocities of each station in the ITRF97 frame (Table D).

An earthquake sequence from September through December, 1994 occurs within the time span of GPS observations. A M_w 7 earthquake occurred Sept. 1, 1994, > 100 km offshore of Cape Mendocino (Dengler et al., 1995). Observed coseismic displacements (Dengler et al., 1995; M.H. Murray, 2000, personal communication) are used to interpolate displacement values for HPGN stations used in this analysis that do not have post-earthquake information (Table E; Appendix Figure 1).

Station velocities are defined relative to a stable North American plate (Table A). North American plate motion is determined in a global GPS-only defined reference frame, REVEL-2000 (Sella et al., 2002). More than 60 GPS stations located on North America are used to define rigid North America motion. The REVEL-2000 reference frame (Sella et al, 2002) differs from plate circuit models (e.g. Nuvel-1, Nuvel-1A: DeMets et al., 1990, 1994; DeMets and Dixon, 1999); geologic plate circuit models are generally ~ 3 Ma averages, whereas REVEL-2000 and this study span the same time period (1993-2000).

Acknowledgements

Initial original GPS measurements come from the California Department of Transportation (CalTrans) (1993; 1994; 1998), the National Geodetic Survey (1994; 1998), Stanford University (1994; 1995; Freymueller et al., 1999) and the U. S. Geological Survey (1996; 1999; 2001; Poland et al., 1999; J.Svarc, 2001, personal

communication). Reoccupation of the initial GPS stations (1999-2002) was performed primarily by Humboldt State University and University of Alaska-Fairbanks (UAF), while field support was provided by CalTrans District 1, Central Washington University (CWU), Lane Community College, and the University of Oregon. GPS equipment support was provided (1999-2002) by the Geodesy Lab at CWU, the Geophysical Institute at UAF, and the University NAVSTAR Consortium (UNAVCO, Boulder, CO). Most benchmarks resurveyed in this study are those of the California High Precision Geodetic Network (HPGN) or High Accuracy Reference Network (HARN) jointly established in 1991 by CalTrans and the NGS. We acknowledge the availability of online archives for precise orbits of satellites as well as global tracking data from continuously recording GPS reference stations available from the Bay Area Regional Deformation network (http://quake.geo.berkeley.edu/bard/bard.html), the International GPS Service (http://igscb.jpl.nasa.gov/components/prods_cb.html), the National Geodetic Survey (http//www.ngs.noaa.gov), the Pacific Northwest Geodetic Array (http//www.geodesy.cwu.edu), and SCRIPPS Orbit and Permanent Array Center (http://sopac.ucsd.edu/).

References Cited

Argus, D. F., Heflin, M. B., Donnellan, A., Webb, F. H., Dong, D., Hurst, K. J., Jefferson, D. C., Lyzenga, G. A., Watkins, M. M., Zumberge, J. F., 1999, Shortening and thickening of metropolitan Los Angeles measured and inferred by using geodesy, Geology, v.27, n. 8, p.703-706.

Boucher, C., Altamini, Z., and Sillard, P., 1999, The 1997 International Terrestrial Reference Frame (ITRF97), in IERS Technical Note 27, Observatoire de Paris, Paris, France.

Clarke, S. H., Jr., and Carver, G. A., 1992, Late Holocene tectonics and paleoseismicity, southern Cascadia subduction zone, Science, v. 255, p. 188-192.

Dengler, L., Moley, K., McPherson, R., Pasyanos, M., Dewey, J. W., Murray, M. H., 1995, The September 1, 1994 Mendocino fault earthquake, California Geology, v. 48, n. 2, p.43-53.

DeMets, C., Gordon, R. G., Argus, D. F., and Stein, S., 1990, Current plate motions, Geophysical Journal International, 101, p. 425-478.

DeMets, C., Gordon, R. G., Argus, D. F., and Stein, S., 1994, Effect of revisions to the geomagnetic time scale on estimates of current plate motion, Geophysical Research Letters, n. 21, p. 2191-2194.

DeMets, C., and Dixon, T. H., 1999, Kinematic models for Pacific-North America motion from 3 Ma to present, I: Evidence for steady motion and biases in the NUVEL-1A model, Geophysical Research Letters, v.26, p. 1921-1924.

Dixon, T. H., Miller, M. M., Farina, F., Wang, H., and Johnson, D. J., 2000, Present-day motion of the Sierra Nevada block and some tectonic implications for the Basin and Range province, North America Cordillera, Tectonics, v. 19, n. 1, p. 1-24.

Flueck, P., Hyndman, R. D., and Wang, K., 1997, Three-dimensional dislocation model for great earthquakes of the Cascadia subduction zone, Journal of Geophysical Research, v. 102, p. 20,539 – 20,550.

Freymueller, J. T., Murray, M. H., Segall, P., and Castillo, D., 1999, Kinematics of the Pacific-North America plate boundary zone, northern California. Journal of Geophysical Research, v.104, no. B4, p. 7419-7441.

Freymueller, J. T., Cohen, S. C., and Fletcher, H. J., 2000, Spatial variations in present-day deformation, Kenai Peninsula, and their implications, Journal of Geophysical Research, v.105, n.4, p.8079-8101.

Jennings, C., 1994, Fault activity map of California and adjacent areas, Department of Conservation, California Division of Mines and Geology, Sacramento, CA.

Kelsey, H. M., and Carver, G. A., 1988, Late Neogene and Quaternary tectonics associated with the northward growth of the San Andreas Transform fault, northern California. Journal of Geophysical Research, v. 93, no. B5, p. 4797- 4819.

McCrory, P. A., 2000, Upper plate contraction north of the migrating Mendocino triple junction, northern California: implications for strain partitioning, Tectonics, v. 19, p. 1144-1160.

Miller, M. M, Wang, K., Qamar, A., Goldfinger, C., Johnson, D.J., Rubin, C.M., and Dragert H., 2001, GPS-determination of along-strike variation in Cascadia margin kinematics: Implications for relative plate motion, subduction zone coupling, and permanent deformation, Tectonics, v. 20, n. 2, p.161-176.

Murray, M. H., Marshall, G. A., Lisowski, M., and Stein, R. S., 1996, The 1992 M=7 Cape Mendocino, California, earthquake: Coseismic deformation at the south end of the Cascadia megathrust, Journal of Geophysical Research, v. 101, n. B8, p. 17,707-17, 725.

Murray, M.H., 2000, personal communication.

Murray, M. H., and Lisowski, M., 2000, Strain accumulation along the Cascadia subduction zone, Geophysical Research Letters, v.27, p. 3631-3634.

Poland, M. P., Burgmann, R., Fink, J. H., and Dzurisin, D., 1999, Deformation field at Medicine Lake Volcano, Northern California; new results from GPS measurements, EOS, Transactions, American Geophysical Union, v. 80, p. 960.

Prescott, W. H., Savage, J. C., Svarc, J. L., and Manaker, D., 2001, Deformation across the Pacific-North America plate boundary near San Francisco, California, Journal of Geophysical Research, v. 106, p. 6673-6682.

Sella, G. F., Dixon, T. H., Mao, A., and Stein, S., 2002, REVEL: A model for Recent plate velocities from space geodesy, Journal of Geophysical Research, v. 107, n. B4, 10.1029/2000JB000033.

Smith, S. W., Knapp, J. S., McPherson, R. C., 1993, Seismicity of the Gorda plate. Structure of the continental margin, and an eastward jump of the Mendocino triple junction, Journal of Geophysical Research, v. 98, p. 8153-8171.

Svarc, J., USGS, Menlo Park, CA, personal communication.

Wilson, D. S., 1993, Confidence intervals for motion and deformation of the Juan de Fuca plate, Journal of Geophysical Research, v. 98, p. 16,053 – 16,071.

Zumberge, J. F., Heflin, M. B., Jefferson, D. C., Watkins, M. M., and Webb, F. H., 1997, Precise point positioning for the efficient and robust analysis of GPS data from large networks, Journal of Geophysical Research, v. 102, p. 5005-5017.

BIBLIOGRAPHY OF PUBLICATIONS RESULTING FROM THE WORK PERFORMED

Williams, T. B., Kelsey, H. M. and Freymueller, J .T., 2002, Escape of Sierra Nevada-Great Valley block motion contributes to upper-plate contraction within the southern Cascadia margin near Humboldt Bay, California, Trans AGU 83(47) Fall Meeting Supplement, Abstract S22B-1028.

Williams, T, B. and Kelsey, H. M. and Freymueller, J. T., 2002, The Geodetic signature of modern deformation w the southern Cascadia margin, northwestern California, Geological Society of American Abstracts with Prog 43, no. 6, p. P-67.

AVAILABILITY OF SEISMIC, GEODETIC, OR PROCESSED DATA.

GPS survey data (RINEX files) currently available upon request (tbw3@axe.humboldt.edu) and from the UNAVCO project archive (http://archive.unavco.ucar.edu/) under the 'Cascadia 2001' project group name. RINEX data from 1999-2001 has been submitted to J. Svarc, USGS, Menlo Park, CA.

Files containing final station velocity estimates, model output, and interpolated coseismic earthquake displacements are also available upon request (tbw3@axe.humboldt.edu).

Williams' M.S. thesis is available as a downloadable .pdf file (~ 45 Mb) from the HSU Geology web page (http://www.humboldt.edu/~geodept/RESEARCH/RESEARCH.HTM). A research project web page will contain all of the pertinent project information in the near future.

Table A. GPS station velocities relative to a fixed North American plate.

Station	Longitude	Latitude	East Vel.	North Vel.	Sigma East	Sigma North	Correlation
4-char ID	degrees	degrees N	cm/yr	cm/yr	cm/yr	cm/yr	east-north
0104	-123.2010	39.7954	-1.19	0.86	0.07	0.05	-0.2025
0105	-123.8352	39.7769	-2.44	2.66	0.07	0.05	-0.2321
0106	-123.5235	40.4602	-0.62	0.85	0.08	0.05	-0.2539
0108	-123.4935	40.8153	-0.42	0.91	0.09	0.07	-0.2877
0109	-124.1174	40.9750	0.36	1.56	0.10	0.07	-0.3057
0110	-123.4759	41.4002	-0.29	0.82	0.17	0.12	0.0245
0113	-124.1584	41.9325	0.26	1.07	0.30	0.20	-0.3939
0201	-123.1930	41.8415	-0.16	0.99	0.22	0.17	0.1056
0202	-122.5913	41.9558	-0.26	0.47	0.26	0.20	0.2065
0208	-122.2750	41.5321	-0.20	0.62	0.17	0.11	-0.2194
0212	-122.4349	40.9571	-0.74	0.56	0.34	0.15	-0.2760
0217	-122.9419	40.6521	-0.63	0.74	0.09	0.07	-0.0859
0220	-120.3665	40.7992	-0.44	0.45	0.18	0.09	-0.0423
0221	-122.9364	40.3696	-0.82	0.62	0.09	0.06	-0.0755
0226	-119.9944	40.2450	-0.53	0.53	0.17	0.09	-0.0467
0229	-122.5768	40.6476	-1.13	0.48	0.26	0.17	-0.3554
0411	-123.0381	38.3240	-2.00	3.17	0.18	0.11	-0.0852
0412	-122.4068	38.4411	-1.01	1.53	0.16	0.09	0.0787
0413	-123.4008	38.6533	-2.47	3.41	0.12	0.07	-0.0568
0414	-122.8121	38.6709	-1.15	2.33	0.14	0.08	-0.0395
1005	-120.2667	37.9972	-1.06	0.35	0.28	0.11	-0.0966
1402	-123.9852	40.8876	0.23	1.33	0.24	0.13	-0.2162
1436	-123.7905	39.6691	-2.08	2.67	0.31	0.12	0.0590
1468	-124.1557	40.4481	-0.66	2.47	0.16	0.07	0.0184
8767	-124.2176	40.7669	0.60	1.94	0.14	0.09	-0.1297
9750	-124.1815	41.7484	0.11	1.01	0.20	0.13	-0.1112
01KD	-123.7945	40.0942	-1.59	2.03	0.19	0.08	0.0472
01LD	-123.8316	40.2508	-1.26	1.77	0.19	0.08	0.0528
01MC	-123.9211	40.3225	-1.09	1.94	0.20	0.08	0.1092
01NC	-124.0330	40.4396	-0.53	2.07	0.20	0.09	0.0300
01ND	-123.7974	40.4721	-0.28	1.57	0.22	0.16	0.1096
01NE	-123.6751	40.4390	-0.80	1.41	0.18	0.06	0.0722
01PA	-124.2556	40.5890	0.00	2.18	0.15	0.09	0.0087
01PB	-124.2034	40.6393	0.29	1.95	0.28	0.15	-0.3681
01QB	-124.1994	40.7447	0.03	1.91	0.26	0.14	-0.3290
01QF	-123.3251	40.8145	-0.41	0.57	0.16	0.09	-0.1372
01RB	-124.0874	40.9065	0.15	1.59	0.23	0.14	-0.0694
01RD	-123.7724	40.8964	-0.50	0.98	0.14	0.07	-0.2192
01RE	-123.6225	40.9439	-0.60	0.99	0.12	0.07	-0.1262

Table A (con't). GPS station velocities relative to fixed North America.

Station	Longitude	Latitude	East Vel.	North Vel.	Sigma East	Sigma North	Correlation
4-char ID	degrees	degrees N	cm/yr	cm/yr	cm/yr	cm/yr	east-north
01T4	-123.6557	41.2405	-1.30	1.24	0.36	0.22	-0.2171
01XD	-123.8443	41.8744	0.28	0.59	0.39	0.25	0.0497
ALEN	-124.0951	41.1917	0.40	1.17	0.16	0.11	0.1622
ALGO	-78.0714	45.9558	-0.04	0.03	0.05	0.03	0.0544
ANDE	-122.2906	40.4195	-1.05	0.74	0.21	0.14	-0.0411
ARP	-124.1158	40.8048	0.17	1.75	0.26	0.17	-0.0533
BLDK	-123.8654	40.8820	-0.34	1.37	0.13	0.08	-0.0053
BRR2	-124.2945	40.4977	-0.68	2.58	0.26	0.08	0.0296
CABL	-124.5633	42.8361	0.71	1.33	0.04	0.03	-0.0262
CME1	-124.3963	40.4418	-0.61	3.05	0.04	0.03	0.0090
CR01	-124.1952	40.6975	-0.41	2.27	0.14	0.09	0.0066
GOL2	-116.8893	35.4252	-0.72	0.58	0.04	0.03	0.0423
GOLD	-116.8893	35.4252	-0.68	0.57	0.04	0.03	0.0405
GREN	-122.5259	41.5550	-0.32	0.36	0.17	0.12	-0.0715
HATC	-121.4713	40.8177	-0.63	0.46	0.14	0.10	-0.3177
HAYF	-123.2187	40.6588	-1.09	0.91	0.23	0.14	0.0046
HOPB	-123.0747	38.9952	-1.82	2.11	0.04	0.03	0.0237
KNEE	-123.9748	40.7266	0.13	1.44	0.12	0.08	-0.5126
MUMB	-122.5326	41.1844	-0.47	0.65	0.07	0.05	-0.0119
NEW2	-117.5089	39.6856	-0.20	0.06	0.04	0.04	0.0107
NLIB	-91.5749	41.7716	-0.03	0.06	0.04	0.03	0.0270
PENT	-119.6250	49.3226	0.20	0.03	0.04	0.04	-0.0872
PILG	-121.9819	41.2597	-0.68	0.57	0.17	0.11	0.0185
PTRB	-123.0187	37.9962	-2.40	3.56	0.07	0.05	0.0234
PTSG	-124.2552	41.7827	0.40	1.14	0.05	0.04	-0.0050
QUIN	-120.9444	39.9746	-0.76	0.69	0.04	0.03	0.0064
ROHN	-124.1318	40.5540	-0.91	1.85	0.31	0.19	-0.0144
SAGE	-120.0388	39.7909	-0.59	0.27	0.13	0.09	-0.0713
SHIN	-120.2250	40.5917	-0.46	0.42	0.04	0.03	0.0032
SHLD	-119.0157	41.8684	-0.27	0.21	0.04	0.04	-0.0063
SUTB	-121.8206	39.2058	-0.95	0.66	0.04	0.03	0.0205
TRND	-124.1509	41.0539	0.52	1.64	0.05	0.04	0.0017
YBHB	-122.7107	41.7317	-0.12	0.65	0.04	0.03	-0.0152

Table B. Model output at observation points.

Station	Longitude	Latitude	East Vel.	North Vel.	Velocity
4-char ID	degrees	degrees N	cm/yr	cm/yr	cm/yr
0104	-123.2010	39.7954	0.00	0.01	0.01
0105	-123.8352	39.7769	-0.02	0.04	0.04
0106	-123.5235	40.4602	0.16	0.03	0.16
0108	-123.4935	40.8153	0.25	0.10	0.27
0109	-124.1174	40.9750	0.69	0.67	0.96
0110	-123.4759	41.4002	0.22	0.11	0.25
0113	-124.1584	41.9325	0.58	0.44	0.72
0201	-123.1930	41.8415	0.14	0.07	0.16
0202	-122.5913	41.9558	0.08	0.04	0.09
0208	-122.2750	41.5321	0.06	0.02	0.07
0212	-122.4349	40.9571	0.06	0.02	0.06
0217	-122.9419	40.6521	0.08	0.02	0.09
0220	-120.3665	40.7992	0.02	0.00	0.02
0221	-122.9364	40.3696	0.05	0.01	0.05
0226	-119.9944	40.2450	0.01	0.00	0.01
0229	-122.5768	40.6476	0.05	0.01	0.05
0411	-123.0381	38.3240	0.00	0.00	0.01
0412	-122.4068	38.4411	0.00	0.00	0.00
0413	-123.4008	38.6533	-0.01	0.01	0.01
0414	-122.8121	38.6709	0.00	0.01	0.01
1005	-120.2667	37.9972	0.00	0.00	0.00
1402	-123.9852	40.8876	0.60	0.47	0.77
1436	-123.7905	39.6691	-0.02	0.03	0.03
1468	-124.1557	40.4481	0.57	0.59	0.82
8767	-124.2176	40.7669	0.84	0.97	1.28
9750	-124.1815	41.7484	0.62	0.52	0.81
01KD	-123.7945	40.0942	-0.02	0.08	0.08
01LD	-123.8316	40.2508	0.00	0.11	0.11
01MC	-123.9211	40.3225	0.06	0.17	0.18
01NC	-124.0330	40.4396	0.40	0.35	0.53
01ND	-123.7974	40.4721	0.29	0.11	0.31
01NE	-123.6751	40.4390	0.20	0.05	0.21
01PA	-124.2556	40.5890	0.89	1.03	1.36
01PB	-124.2034	40.6393	0.83	0.93	1.25
01QB	-124.1994	40.7447	0.82	0.93	1.24
01QF	-123.3251	40.8145	0.18	0.06	0.19
01RB	-124.0874	40.9065	0.68	0.64	0.93
01RD	-123.7724	40.8964	0.44	0.24	0.50
01RE	-123.6225	40.9439	0.32	0.15	0.36

Table B (con't). Model output at observation points.

Station name	Longitude degrees	Latitude degrees	East Vel. cm/yr	North Vel. cm/yr	Velocity (cm/yr)
01T4	-123.6557	41.2405	0.30	0.16	0.35
01XD	-123.8443	41.8744	0.34	0.20	0.39
ALEN	-124.0951	41.1917	0.63	0.55	0.84
ALGO	-78.0714	45.9558	0.00	0.00	0.00
ANDE	-122.2906	40.4195	0.03	0.01	0.03
ARP	-124.1158	40.8048	0.72	0.73	1.02
BLDK	-123.8654	40.8820	0.52	0.32	0.61
BRR2	-124.2945	40.4977	0.90	0.99	1.34
CABL	-124.5633	42.8361	0.85	1.00	1.32
CME1	-124.3963	40.4418	0.98	1.01	1.40
CR01	-124.1952	40.6975	0.82	0.92	1.23
GOL2	-116.8893	35.4252	0.00	0.00	0.00
GOLD	-116.8893	35.4252	0.00	0.00	0.00
GREN	-122.5259	41.5550	0.08	0.03	0.08
HATC	-121.4713	40.8177	0.03	0.01	0.03
HAYF	-123.2187	40.6588	0.13	0.03	0.13
HOPB	-123.0747	38.9952	-0.01	0.01	0.01
KNEE	-123.9748	40.7266	0.59	0.46	0.75
MUMB	-122.5326	41.1844	0.07	0.02	0.08
NEW2	-117.5089	39.6856	0.01	0.00	0.01
NLIB	-91.5749	41.7716	0.00	0.00	0.00
PENT	-119.6250	49.3226	0.04	0.02	0.04
PILG	-121.9819	41.2597	0.05	0.01	0.05
PTRB	-123.0187	37.9962	0.00	0.00	0.00
PTSG	-124.2552	41.7827	0.67	0.64	0.93
QUIN	-120.9444	39.9746	0.01	0.00	0.01
ROHN	-124.1318	40.5540	0.70	0.71	1.00
SAGE	-120.0388	39.7909	0.01	0.00	0.01
SHIN	-120.2250	40.5917	0.01	0.00	0.01
SHLD	-119.0157	41.8684	0.02	0.00	0.02
SUTB	-121.8206	39.2058	0.00	0.00	0.00
TRND	-124.1509	41.0539	0.70	0.71	0.99
YBHB	-122.7107	41.7317	0.09	0.04	0.10

Table C. Residual station velocities.

Site	Longitude	Latitude	East Vel.	North Vel.	Sigma East	Sigma North	Correlation
4-char ID	degrees	degrees N	cm/yr	cm/yr	cm/yr	cm/yr	east-north
0104	-123.2010	39.7954	-1.19	0.85	0.07	0.05	-0.2025
0105	-123.8352	39.7769	-2.42	2.62	0.07	0.05	-0.2321
0106	-123.5235	40.4602	-0.78	0.82	0.08	0.05	-0.2539
0108	-123.4935	40.8153	-0.67	0.81	0.09	0.07	-0.2877
0109	-124.1174	40.9750	-0.33	0.89	0.10	0.07	-0.3057
0110	-123.4759	41.4002	-0.51	0.71	0.17	0.12	0.0245
0113	-124.1584	41.9325	-0.32	0.64	0.30	0.20	-0.3939
0201	-123.1930	41.8415	-0.31	0.91	0.22	0.17	0.1056
0202	-122.5913	41.9558	-0.35	0.44	0.26	0.20	0.2065
0208	-122.2750	41.5321	-0.27	0.60	0.17	0.11	-0.2194
0212	-122.4349	40.9571	-0.80	0.55	0.34	0.15	-0.2760
0217	-122.9419	40.6521	-0.72	0.72	0.09	0.07	-0.0859
0220	-120.3665	40.7992	-0.46	0.45	0.18	0.09	-0.0423
0221	-122.9364	40.3696	-0.87	0.61	0.09	0.06	-0.0755
0226	-119.9944	40.2450	-0.54	0.53	0.17	0.09	-0.0467
0229	-122.5768	40.6476	-1.18	0.47	0.26	0.17	-0.3554
0411	-123.0381	38.3240	-2.00	3.16	0.18	0.11	-0.0852
0412	-122.4068	38.4411	-1.00	1.52	0.16	0.09	0.0787
0413	-123.4008	38.6533	-2.47	3.40	0.12	0.07	-0.0568
0414	-122.8121	38.6709	-1.14	2.32	0.14	0.08	-0.0395
1005	-120.2667	37.9972	-1.06	0.35	0.28	0.11	-0.0966
1402	-123.9852	40.8876	-0.38	0.86	0.24	0.13	-0.2162
1436	-123.7905	39.6691	-2.06	2.64	0.31	0.12	0.0590
1468	-124.1557	40.4481	-1.24	1.88	0.16	0.07	0.0184
8767	-124.2176	40.7669	-0.24	0.97	0.14	0.09	-0.1297
9750	-124.1815	41.7484	-0.51	0.49	0.20	0.13	-0.1112
01KD	-123.7945	40.0942	-1.56	1.96	0.19	0.08	0.0472
01LD	-123.8316	40.2508	-1.26	1.66	0.19	0.08	0.0528
01MC	-123.9211	40.3225	-1.15	1.77	0.20	0.08	0.1092
01NC	-124.0330	40.4396	-0.92	1.72	0.20	0.09	0.0300
01ND	-123.7974	40.4721	-0.57	1.45	0.22	0.16	0.1096
01NE	-123.6751	40.4390	-1.00	1.36	0.18	0.06	0.0722
01PA	-124.2556	40.5890	-0.89	1.15	0.15	0.09	0.0087
01PB	-124.2034	40.6393	-0.53	1.02	0.28	0.15	-0.3681
01QB	-124.1994	40.7447	-0.79	0.98	0.26	0.14	-0.3290
01QF	-123.3251	40.8145	-0.59	0.51	0.16	0.09	-0.1372
01RB	-124.0874	40.9065	-0.53	0.95	0.23	0.14	-0.0694
01RD	-123.7724	40.8964	-0.93	0.74	0.14	0.07	-0.2192
01RE	-123.6225	40.9439	-0.92	0.84	0.12	0.07	-0.1262

Table C (con't). Residual station velocities.

Site	Longitude	Latitude	East Vel.	North Vel.	Sigma East	Sigma North	Correlation
4-char ID	degrees	degrees N	cm/yr	cm/yr	cm/yr	cm/yr	east-north
01T4	-123.6557	41.2405	-1.60	1.08	0.36	0.22	-0.2171
01XD	-123.8443	41.8744	-0.06	0.39	0.39	0.25	0.0497
ALEN	-124.0951	41.1917	-0.23	0.62	0.16	0.11	0.1622
ALGO	-78.0714	45.9558	-0.04	0.03	0.05	0.03	0.0544
ANDE	-122.2906	40.4195	-1.08	0.73	0.21	0.14	-0.0411
ARP	-124.1158	40.8048	-0.55	1.02	0.26	0.17	-0.0533
BLDK	-123.8654	40.8820	-0.86	1.04	0.13	0.08	-0.0053
BRR2	-124.2945	40.4977	-1.58	1.59	0.26	0.08	0.0296
CABL	-124.5633	42.8361	-0.14	0.33	0.04	0.03	-0.0262
CME1	-124.3963	40.4418	-1.59	2.04	0.04	0.03	0.0090
CR01	-124.1952	40.6975	-1.23	1.35	0.14	0.09	0.0066
GOL2	-116.8893	35.4252	-0.72	0.58	0.04	0.03	0.0423
GOLD	-116.8893	35.4252	-0.68	0.57	0.04	0.03	0.0405
GREN	-122.5259	41.5550	-0.39	0.33	0.17	0.12	-0.0715
HATC	-121.4713	40.8177	-0.66	0.45	0.14	0.10	-0.3177
HAYF	-123.2187	40.6588	-1.22	0.88	0.23	0.14	0.0046
HOPB	-123.0747	38.9952	-1.81	2.10	0.04	0.03	0.0237
KNEE	-123.9748	40.7266	-0.46	0.98	0.12	0.08	-0.5126
MUMB	-122.5326	41.1844	-0.54	0.62	0.07	0.05	-0.0119
NEW2	-117.5089	39.6856	-0.20	0.06	0.04	0.04	0.0107
NLIB	-91.5749	41.7716	-0.03	0.06	0.04	0.03	0.0270
PENT	-119.6250	49.3226	0.17	0.01	0.04	0.04	-0.0872
PILG	-121.9819	41.2597	-0.72	0.56	0.17	0.11	0.0185
PTRB	-123.0187	37.9962	-2.39	3.56	0.07	0.05	0.0234
PTSG	-124.2552	41.7827	-0.27	0.51	0.05	0.04	-0.0050
QUIN	-120.9444	39.9746	-0.77	0.68	0.04	0.03	0.0064
ROHN	-124.1318	40.5540	-1.61	1.14	0.31	0.19	-0.0144
SAGE	-120.0388	39.7909	-0.60	0.26	0.13	0.09	-0.0713
SHIN	-120.2250	40.5917	-0.48	0.42	0.04	0.03	0.0032
SHLD	-119.0157	41.8684	-0.28	0.20	0.04	0.04	-0.0063
SUTB	-121.8206	39.2058	-0.95	0.65	0.04	0.03	0.0205
TRND	-124.1509	41.0539	-0.18	0.93	0.05	0.04	0.0017
YBHB	-122.7107	41.7317	-0.21	0.61	0.04	0.03	-0.0152

Table D. GPS station velocities in the ITRF97 reference frame.

Station	Longitude	Latitude	East Vel.	North Vel.	Sigma East	Sigma North	Correlation
4-char ID	degrees	degrees N	cm/yr	cm/yr	cm/yr	cm/yr	east-north
0104	-123.2010	39.7954	-2.27	-0.68	0.07	0.05	-0.2016
0105	-123.8352	39.7769	-3.51	1.10	0.07	0.05	-0.2326
0106	-123.5235	40.4602	-1.71	-0.70	0.08	0.05	-0.2565
0108	-123.4935	40.8153	-1.52	-0.64	0.09	0.06	-0.2903
0109	-124.1174	40.9750	-0.73	0.00	0.10	0.06	-0.3090
0110	-123.4759	41.4002	-1.40	-0.72	0.17	0.12	0.0261
0113	-124.1584	41.9325	-0.85	-0.50	0.30	0.20	-0.3946
0201	-123.1930	41.8415	-1.29	-0.56	0.22	0.17	0.1068
0202	-122.5913	41.9558	-1.40	-1.05	0.26	0.20	0.2076
0208	-122.2750	41.5321	-1.34	-0.89	0.17	0.11	-0.2199
0212	-122.4349	40.9571	-1.86	-0.96	0.34	0.15	-0.2766
0217	-122.9419	40.6521	-1.74	-0.80	0.09	0.07	-0.0830
0220	-120.3665	40.7992	-1.60	-1.01	0.18	0.09	-0.0412
0221	-122.9364	40.3696	-1.92	-0.91	0.09	0.06	-0.0719
0226	-119.9944	40.2450	-1.67	-0.92	0.17	0.09	-0.0454
0229	-122.5768	40.6476	-2.24	-1.04	0.26	0.16	-0.3561
0411	-123.0381	38.3240	-3.06	1.63	0.18	0.11	-0.0838
0412	-122.4068	38.4411	-2.08	0.01	0.16	0.09	0.0825
0413	-123.4008	38.6533	-3.53	1.86	0.12	0.07	-0.0530
0414	-122.8121	38.6709	-2.21	0.80	0.14	0.08	-0.0364
1005	-120.2667	37.9972	-2.15	-1.11	0.28	0.11	-0.0961
1402	-123.9852	40.8876	-0.86	-0.23	0.24	0.13	-0.2166
1436	-123.7905	39.6691	-3.15	1.12	0.31	0.12	0.0604
1468	-124.1557	40.4481	-1.74	0.91	0.16	0.07	0.0218
8767	-124.2176	40.7669	-0.49	0.37	0.14	0.09	-0.1288
9750	-124.1815	41.7484	-1.00	-0.56	0.20	0.13	-0.1108
01KD	-123.7945	40.0942	-2.67	0.47	0.18	0.08	0.0506
01LD	-123.8316	40.2508	-2.34	0.21	0.19	0.08	0.0562
01MC	-123.9211	40.3225	-2.17	0.38	0.20	0.08	0.1129
01NC	-124.0330	40.4396	-1.61	0.51	0.20	0.09	0.0323
01ND	-123.7974	40.4721	-1.37	0.01	0.22	0.16	0.1111
01NE	-123.6751	40.4390	-1.89	-0.15	0.18	0.06	0.0774
01PA	-124.2556	40.5890	-1.08	0.61	0.15	0.09	0.0113
01PB	-124.2034	40.6393	-0.79	0.38	0.28	0.15	-0.3691
01QB	-124.1994	40.7447	-1.06	0.34	0.26	0.14	-0.3298
01QF	-123.3251	40.8145	-1.52	-0.97	0.16	0.09	-0.1369
01RB	-124.0874	40.9065	-0.95	0.02	0.23	0.14	-0.0687
01RD	-123.7724	40.8964	-1.59	-0.58	0.14	0.07	-0.2205
01RE	-123.6225	40.9439	-1.70	-0.56	0.12	0.07	-0.1252

Table D (con't). GPS station velocities in the ITRF97 reference frame.

Station	Longitude	Latitude	East Vel.	North Vel.	Sigma East	Sigma North	Correlation
4-char ID	degrees	degrees N	cm/yr	cm/yr	cm/yr	cm/yr	east-north
01T4	-123.6557	41.2405	-2.40	-0.31	0.36	0.22	-0.2172
01XD	-123.8443	41.8744	-0.84	-0.97	0.39	0.25	0.0500
ALEN	-124.0951	41.1917	-0.70	-0.40	0.16	0.11	0.1655
ALGO	-78.0714	45.9558	-1.69	0.07	0.04	0.03	0.0618
ANDE	-122.2906	40.4195	-2.17	-0.78	0.21	0.14	-0.0402
ARP	-124.1158	40.8048	-0.92	0.18	0.26	0.17	-0.0527
BLDK	-123.8654	40.8820	-1.44	-0.19	0.13	0.08	-0.0022
BRR2	-124.2945	40.4977	-1.75	1.01	0.26	0.08	0.0319
CABL	-124.5633	42.8361	-0.41	-0.25	0.04	0.03	-0.0080
CME1	-124.3963	40.4418	-1.69	1.47	0.04	0.03	0.0399
CR01	-124.1952	40.6975	-1.50	0.70	0.14	0.09	0.0094
GOL2	-116.8893	35.4252	-1.81	-0.78	0.03	0.03	0.0877
GOLD	-116.8893	35.4252	-1.77	-0.79	0.03	0.03	0.0883
GREN	-122.5259	41.5550	-1.45	-1.16	0.17	0.12	-0.0708
HATC	-121.4713	40.8177	-1.77	-1.03	0.14	0.09	-0.3194
HAYF	-123.2187	40.6588	-2.19	-0.63	0.23	0.14	0.0056
HOPB	-123.0747	38.9952	-2.89	0.57	0.04	0.03	0.0622
KNEE	-123.9748	40.7266	-0.96	-0.12	0.12	0.08	-0.5179
MUMB	-122.5326	41.1844	-1.59	-0.87	0.07	0.05	-0.0038
NEW2	-117.5089	39.6856	-1.37	-1.31	0.04	0.03	0.0298
NLIB	-91.5749	41.7716	-1.53	-0.42	0.04	0.03	0.0283
PENT	-119.6250	49.3226	-1.13	-1.41	0.03	0.03	-0.1091
PILG	-121.9819	41.2597	-1.81	-0.93	0.17	0.11	0.0201
PTRB	-123.0187	37.9962	-3.45	2.03	0.07	0.05	0.0379
PTSG	-124.2552	41.7827	-0.70	-0.43	0.05	0.03	0.0140
QUIN	-120.9444	39.9746	-1.88	-0.79	0.03	0.03	0.0377
ROHN	-124.1318	40.5540	-1.99	0.28	0.31	0.19	-0.0138
SAGE	-120.0388	39.7909	-1.73	-1.19	0.13	0.09	-0.0697
SHIN	-120.2250	40.5917	-1.61	-1.03	0.04	0.03	0.0252
SHLD	-119.0157	41.8684	-1.46	-1.21	0.04	0.03	0.0065
SUTB	-121.8206	39.2058	-2.04	-0.85	0.04	0.03	0.0529
TRND	-124.1509	41.0539	-0.57	0.07	0.05	0.03	0.0237
YBHB	-122.7107	41.7317	-1.25	-0.88	0.04	0.03	0.0048

Table E. Displacements related to the 1994 offshore M=7 Mendocino fault earthquake (Appendix Figure 1).

USGS GPS station displacements after the 1994 Mendocino earthquake (Dengler et al., 1995).

Station	Longitude	Latitude	East Vel.	North Vel.	Sigma East	Sigma North	Correlation
4-char ID	degrees	degrees N	cm/yr	cm/yr	cm/yr	cm/yr	east-north
0107	-124.1412	40.4512	1.86	0.45	0.18	0.18	-0.052
0109	-124.1174	40.9750	1.59	0.58	0.18	0.18	-0.059
ALDE	-123.6932	40.1203	0.60	-0.40	0.10	0.10	-0.052
BLDK	-123.8654	40.8820	1.02	-0.01	0.18	0.17	-0.062
BRR2	-124.2945	40.4977	1.70	0.71	0.10	0.08	0.014
COOS	-124.2660	40.2568	0.98	0.78	0.18	0.20	-0.088
GRSH	-123.9778	40.3064	1.17	0.31	0.27	0.25	-0.132
HORS	-123.7330	40.8747	1.47	0.19	0.18	0.18	-0.071
IAQ2	-123.8826	40.6690	-0.24	0.96	0.18	0.18	-0.085
LASS	-123.5545	40.3340	-0.13	0.00	0.18	0.18	-0.098
PRCE	-124.1200	40.4164	0.78	0.57	0.19	0.19	-0.259
ROHN	-124.1188	40.5589	1.83	0.45	0.17	0.17	-0.076
SCHL	-123.8820	41.1534	1.64	-0.61	0.29	0.27	-0.006
SIS3	-124.2020	40.7154	1.92	0.32	0.31	0.27	0.006
TABL	-124.1937	40.6303	0.90	-0.12	0.14	0.13	-0.021

Interpolated HPGN GPS station displacements from the observed USGS GPS stations.

Station	Longitude	Latitude	East Vel.	North Vel.	Sigma East	Sigma North	Correlation
4-char ID	degrees	degrees N	cm/yr	cm/yr	cm/yr	cm/yr	east-north
1402	-123.9852	40.8876	1.29	0.18	0.19	0.20	-0.0521
1468	-124.1556	40.4481	1.83	0.52	0.17	0.17	-0.0487
01LD	-123.8316	40.2508	0.90	-0.02	0.19	0.20	-0.102
01MC	-123.9211	40.3225	1.09	0.11	0.24	0.26	-0.1261
01NC	-124.0330	40.4396	1.50	-0.03	0.21	0.22	-0.1047
01ND	-123.7974	40.4721	-0.23	-0.77	0.20	0.20	-0.1005
01NE	-123.6751	40.4390	0.05	-0.40	0.18	0.18	-0.0952
01PA	-124.2556	40.5890	1.82	0.56	0.16	0.19	0.0095
01PB	-124.2033	40.6392	1.20	-0.04	0.16	0.18	-0.012
01QB	-124.1994	40.7446	1.70	0.59	0.17	0.18	-0.0179
01RB	-124.0873	40.9064	1.54	0.44	0.20	0.21	-0.0467
01RD	-123.7724	40.8963	1.39	0.12	0.18	0.19	-0.0643
ARP	-124.1157	40.8048	1.67	0.30	0.23	0.26	-0.0217

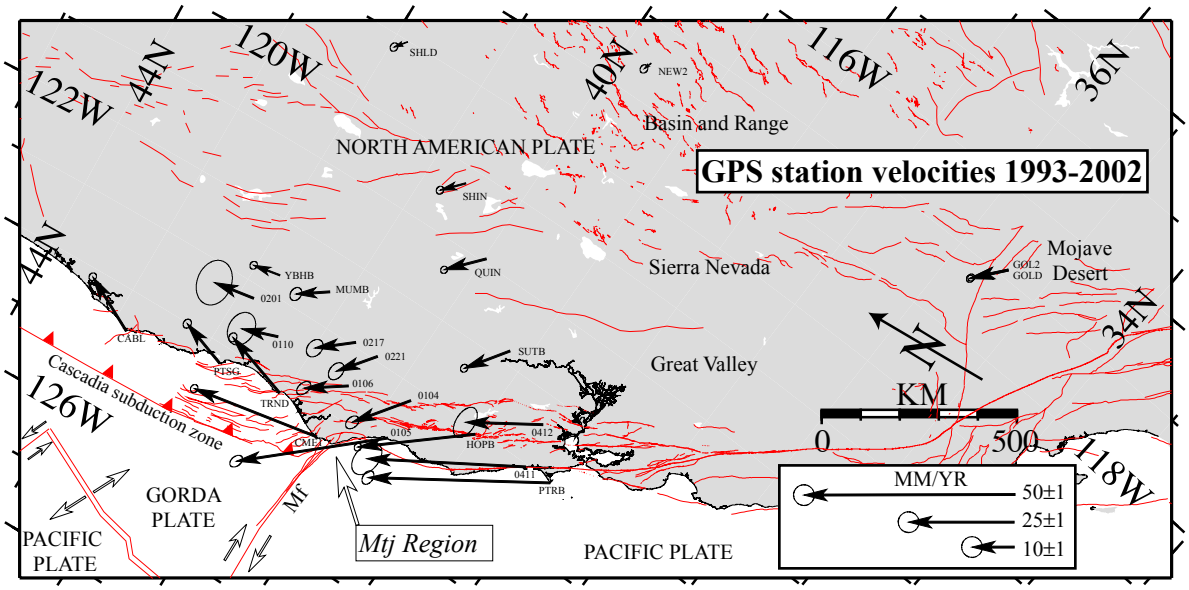

Figure 1. Oblique Mercator projection of the Western U.S. about a pole of rotation determined for observed Pacific-North America relative plate motion (Sella et al., 2002). The long axis is parallel to the direction of P-NA relative motion. Selected GPS station velocities (1993-2002) are shown with respect to a fixed North American plate reference (Table A; Sella et al., 2002). Uncertainty ellipses tip the velocity vectors and are shown for the 2-sigma (95%) confidence interval. Mapped faults (Jennings, 1994) are shown as red lines. The barbed fault represents the Cascadia megathrust. Mf, Mendocino fault; Mtj, Mendocino triple junction.

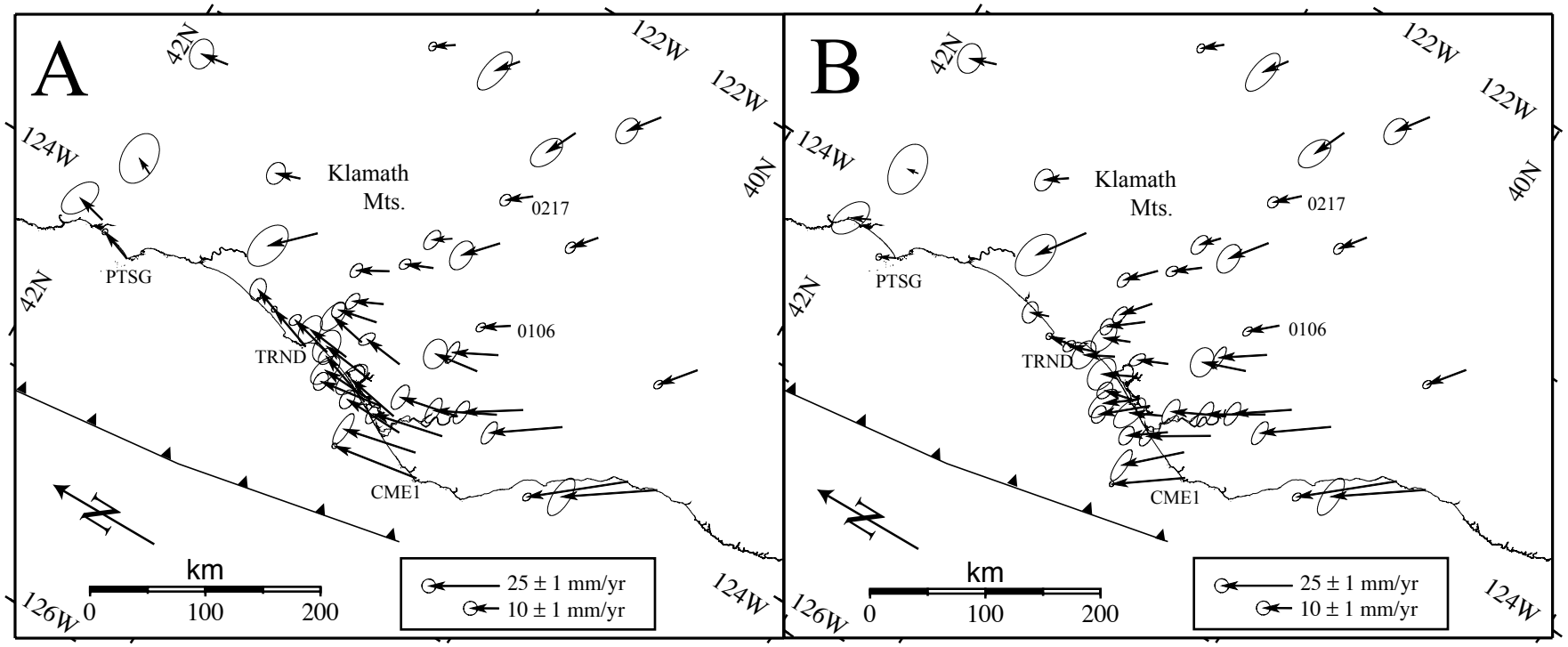

Figure 2. Oblique Mercator projection of the southern Cascadia subduction zone about a P-NA pole of rotation (Sella et al., 2002). The long axis is parallel to the direction of P-NA relative motion. A) Observed GPS station velocities (1993-2002). B) Residual velocities after subtracting the model estimates of interseismic strain accumulation on the southern Cascadia subduction zone (Flueck et al., 1997). The velocity field in (B) reflects the contribution of external forces acting on the southern Cascadia subduction zone other than subduction. The residual velocities are predominately sub-parallel to the Sierra Nevada- Great Valley block and the direction of P-NA relative motion along the northern San Andreas fault system. The barbed fault represents the model fault (Flueck et al., 1997) used in this analysis.

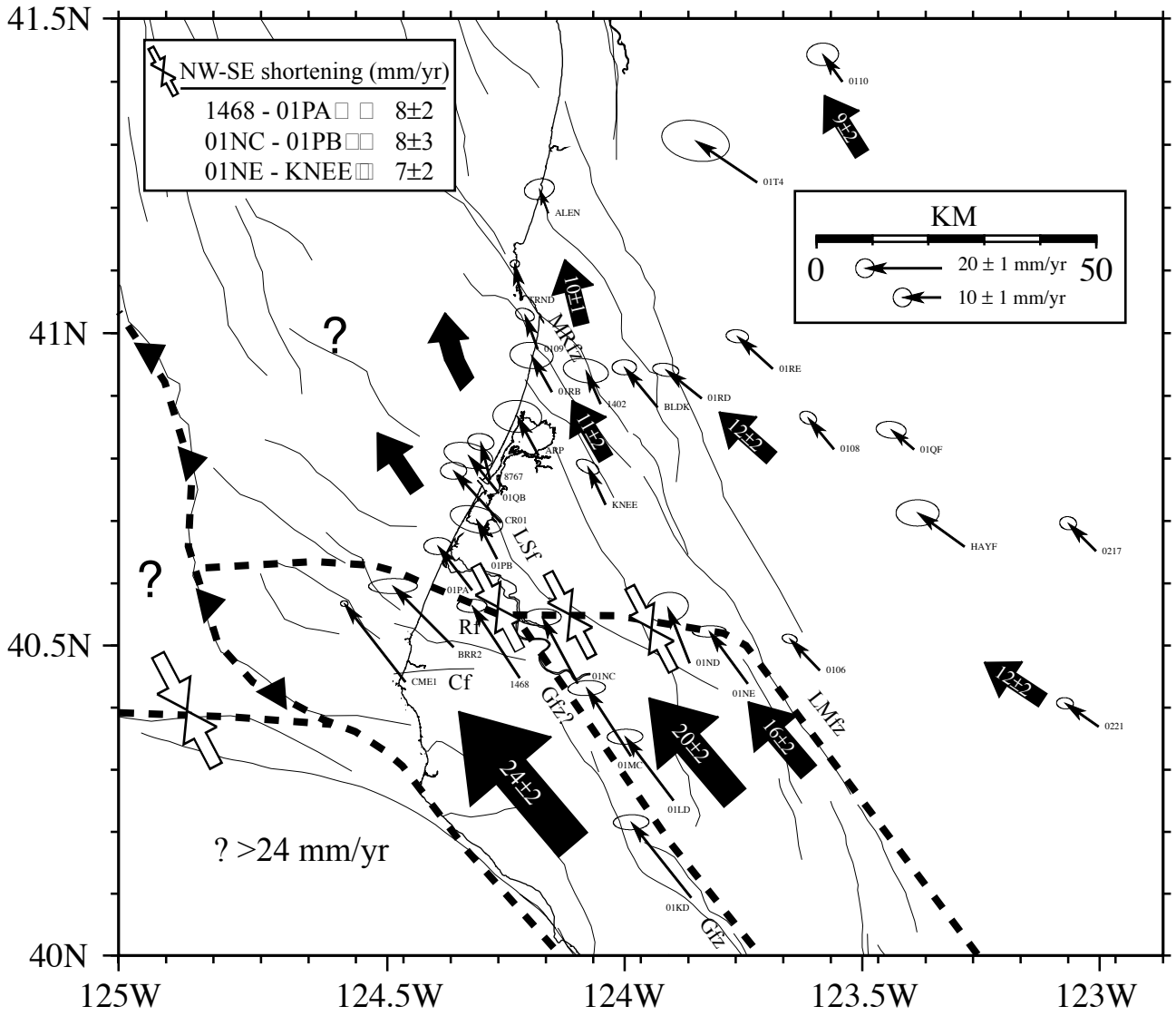

Figure 3. Residual velocities and estimates of long term deformation. With model estimates of the subduction zone removed, the residual velocities provide an image of the differential deformation that occurs as the triple junction region migrates northward. The motion of adjacent stations is generalized using the schematic arrows and average rates of deformation, and depicts that the current configuration of the triple junction region may be comprised of blocks that accommodate regional deformation associated with passage of the Mendocino triple junction.

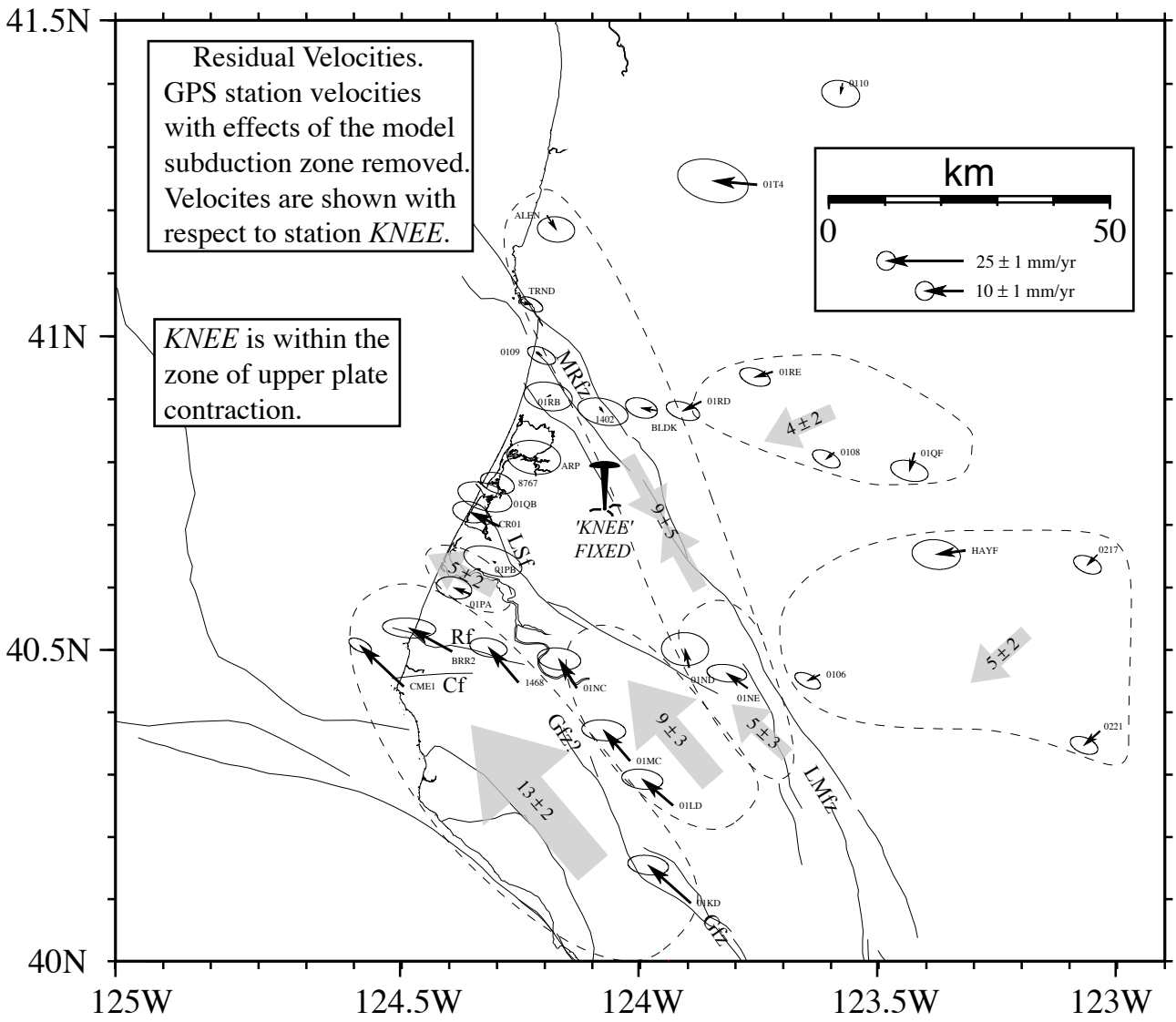

Figure 4. Residual velocities with respect to station KNEE. Shaded velocity arrows are averages of the velocities within dashed boundaries. Relative to a station within the zone of upper plate contraction (KNEE), the residual velocities describe additional NE-SW contraction between the coast and regions inland, as well as NW-SE contraction parallel to the direction of P-NA motion. Although the inland region is moving toward the coast, site specific shortening across the Mad River fault zone (MRfz) cannot be detected. Distributed dextral translational deformation occurs across the northern San Andreas fault system, with velocity increases evident across traces of the Garberville fault zone (Gfz) and the Lake Mountain fault zone (LMfz). Cf, Capetown fault; Rf, Russ fault.

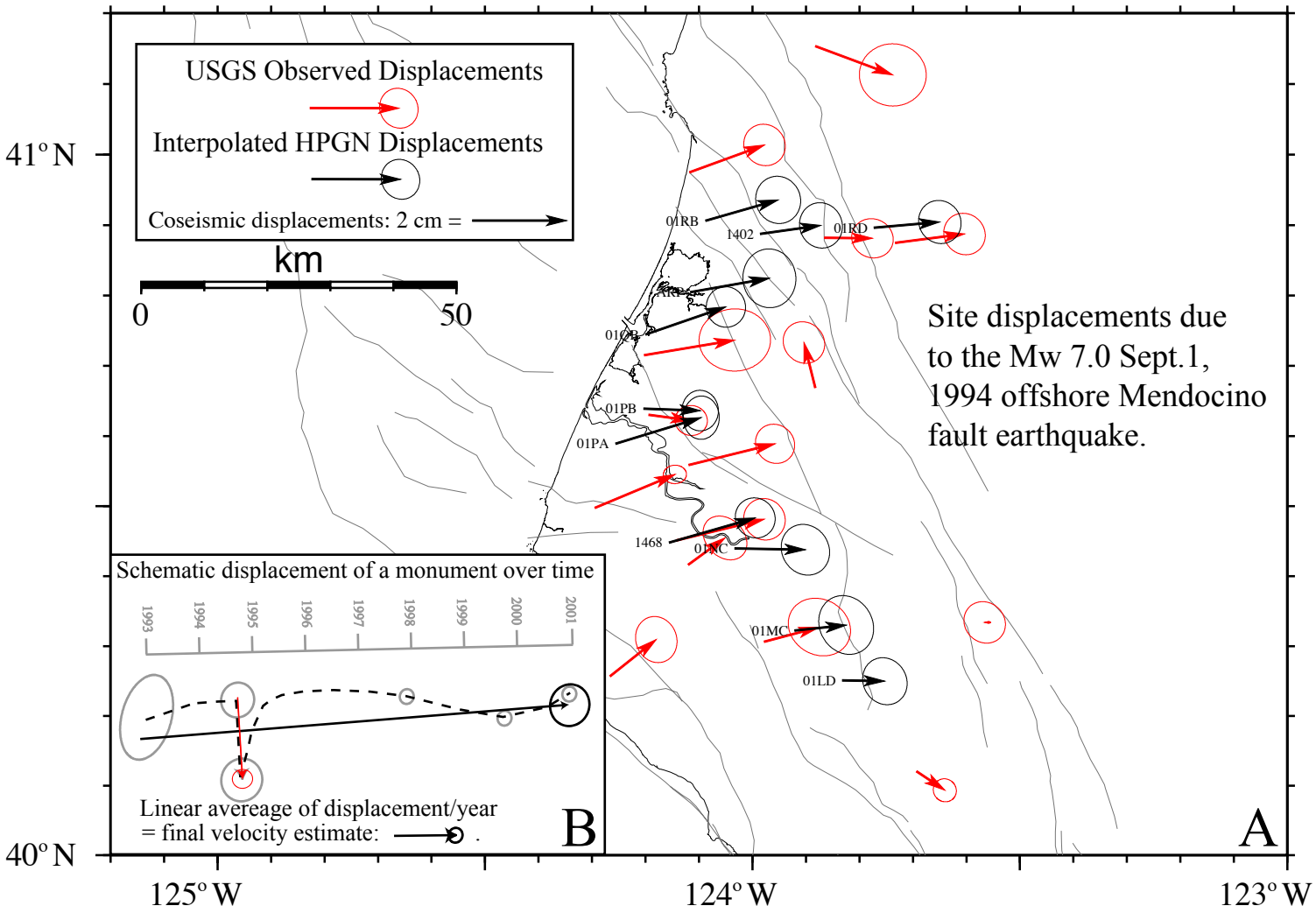

Appendix Figure 1. Observed (Dengler, et al., 1995; M.H. Murray, 2000, personal communication) and interpolated GPS station displacements related to the 1994 offshore M=7 Mendocino fault earthquake.